Unsupervised blind deconvolution

Roberto Baena Gallé

University of Barcelona, c\Marti I Franqués 1, 08025 Barcelona, Spain

Royal Academy of Sciences and Arts of Barcelona, Rambla dels Estudis 115, 08002 Barcelona, Spain

Fraunhofer Institute of Optronics, System Technologies and Image Exploitation, Gutleuthausstr. 1, 76275 Ettlingen, Germany

Szymon Gladysz

Fraunhofer Institute of Optronics, System Technologies and Image Exploitation, Gutleuthausstr. 1, 76275 Ettlingen, Germany

Laurent Mugnier

ONERA/DOTA (Département d'Optique Théorique et Appliquée), B.P. 72, 92322 Châtillon cedex, France

Rao Gudimetla, Robert L. Johnson, Lee Kann

Air Force Research Laboratory, Directed Energy Directorate, Kirtland AFB, NM, USA

ABSTRACT

To reduce the influence of atmospheric turbulence on images of space-based objects we are developing a maximum *a posteriori* deconvolution approach. In contrast to techniques found in the literature, we are focusing on the statistics of the point-spread function (PSF) instead of the object. We incorporated statistical information about the PSF into multi-frame blind deconvolution. Theoretical constraints on the average PSF shape come from the work of D. L. Fried while for the univariate speckle statistics we rely on the gamma distribution adopted from radar/laser speckle studies of J. W. Goodman. Our aim is to develop deconvolution strategy which is reference-less, i.e., no calibration PSF is required, extendable to longer exposures, and applicable to imaging with adaptive optics. The theory and resulting deconvolution framework were validated using simulations and real data from the 3.5m telescope at the Starfire Optical Range (SOR) in New Mexico.

1. INTRODUCTION

Solutions to recovery of high-resolution images when observing through atmospheric turbulence usually fall into the software ("post-processing") or the hardware (adaptive optics, interferometry) category or the combination of both. Even with very expensive adaptive optics (AO) systems it is necessary to use deconvolution (image reconstruction) to remove image blurring completely [1,2].

Successful restoration of images degraded by atmospheric turbulence was first achieved using the so-called speckle imaging techniques [3]. Speckle imaging works because average short-exposure power spectrum has non-negligible spectral content up to the telescope's diffraction limit D/λ [4]. On the other hand, for long exposures average optical transfer function (OTF) quickly drops to values below the noise limit above the cut-off r_0/λ. No information can be recovered from the part of the spectrum where signal-to-noise ratio (SNR) falls below unity. It is this SNR cutoff that actually determines available resolution, with or without deconvolution, and the SNR cutoff is nearly always short of the diffraction cutoff [5]. Therefore, deconvolution of long-exposure images taken without AO cannot result in reliable amplification of the high-frequency content.

Multi-frame blind deconvolution (MFBD) [6-8] is an image reconstruction method relying on the availability of several images of an object. In addition, many of the MFBD algorithms rely on short exposures for the reason stated above. The multiplicity of image frames acts as an implied constraint because the object is common to every image,

while noise and turbulence fluctuations vary randomly between frames [5]. Even with this advantage, MFBD can get easily trapped in local minima [9].

Regularization is the most popular approach to balancing resolution enhancement and amplification of noise. Early termination of the iterative process or an additional spectral filter can be thought of as simple regularization methods [5]. In our work we rely on the Bayesian formulation of the problem of finding a true object **o** and a (stochastic) PSF **h** which together with noise generated the recorded data **i**:

$$p(\mathbf{o},\mathbf{h}\,|\,\mathbf{i}) = \frac{p(\mathbf{i}\,|\,\mathbf{o},\mathbf{h})\cdot p(\mathbf{o})\cdot p(\mathbf{h})}{p(\mathbf{i})} \tag{1}$$

The theorem states that the conditional probability of the object being equal to **o** and the PSF being equal to **h** given that we recorded data **i** is equal to the product of: conditional probability of the data taking on the value(s) **i** given **o** and **h**, probability of the object being equal to **o**, and the probability of the PSF being equal to **h**, divided by the probability of obtaining the data **i** which is always taken to be unity. In the maximum *a posteriori* (MAP) framework one finds estimates for the object, $\hat{\mathbf{o}}$, and the PSF(s), $\hat{\mathbf{h}}$, which jointly maximize $p(\mathbf{o},\mathbf{h}|\,\mathbf{i})$:

$$[\hat{\mathbf{o}},\hat{\mathbf{h}}] = \arg\max_{\mathbf{o},\,\mathbf{h}} p(\mathbf{o},\mathbf{h}|\,\mathbf{i}) = \arg\max_{\mathbf{o},\,\mathbf{h}} p(\mathbf{i}|\,\mathbf{o},\mathbf{h})\times p(\mathbf{o})\times p(\mathbf{h}) \tag{2}$$

It is often useful to rewrite the above equation in terms of the negative log-likelihoods. Then, $\hat{\mathbf{o}}$ can be defined as the object that minimizes a compound criterion $J_{o,h}(\mathbf{i})$:

$$J_{o,h}(\mathbf{i}) = J_i(\mathbf{o},\mathbf{h}) + J_o(\mathbf{o}) + J_h(\mathbf{h}) \tag{3}$$

where the negative log-likelihoods are defined according to the rule $J_{x,y}(\mathbf{z}) = -\ln p(\mathbf{x},\mathbf{y}|\,\mathbf{z})$. Since a probability density function $p(\mathbf{o})$ for the object is in general not known, solutions in the form of functions with desirable mathematical properties (e.g. noise suppression, edge enhancement) are often used. As these *ad hoc* formulas are not real probability density functions (PDFs), regularization parameters must be used to balance their influence on the cost function in Equation (2). Often these parameters have to be chosen manually [1,8]. Apart from the problem of choosing the right value for them, the mere form of the prior (e.g. an object's power spectral density) could be applicable only to a limited class of real objects, although the object's power spectral density could be estimated from the images themselves [10].

For these reasons we focus on PSF statistics $p(\mathbf{h})$. This part of Equation (2) was almost always removed from the MAP approach [7,10]. Formulas for wavefront statistics and, by extension, for short-exposure PSF statistics have been used in the field of wavefront reconstruction and deconvolution from wavefront sensing [11] but not in the field of image restoration. The few papers which deal with the PSF prior do so for the case of very long exposures [1,12]. Here we present ideas on how to incorporate the body of knowledge about turbulence-induced statistics of intensity into the MAP framework.

2. CONSTRAINTS ON THE TURBULENT PSF

There exists a great deal of theoretical information about the turbulent PSF that has not yet been used in multi-frame blind deconvolution. For example, average ensemble PSF is completely specified by known optical parameters, such as observing wavelength and the aperture of the sensor, and one unknown parameter describing the integrated effect of the atmospheric turbulence between the source and the observer. The often-used parameterization of this integrated effect is through the Fried's coherence length r_0 [13]. If r_0 at the time of the observations could be measured then it could be used to generate an average PSF for subsequent deconvolution. As mentioned in the introduction, deconvolution of the average long-exposure image, even with the perfectly known PSF, cannot result

in a diffraction-limited image when SNR is below unity for high spatial frequencies. Unfortunately, this is very often the case for faint space objects.

On the other hand, short exposures allow the recovery of the diffraction-limited image. Additionally, a sequence of short exposures of an arbitrary object can be processed to yield r_0. In order to remove the object being viewed from the image formation equation an object-cancelling transformation is used [14]. Recently, we proposed an original transformation, which we call "Fourier contrast" method [15]. Here we give a brief description how it works.

Image formation equation, expressed in the Fourier domain, is:

$$\mathbf{I}(\vec{u}) = \mathbf{O}(\vec{u})\mathbf{H}(\vec{u}) \tag{4}$$

where $\vec{u}$ is a spatial frequency vector in the Fourier plane and $\mathbf{I}(\vec{u})$, $\mathbf{O}(\vec{u})$ and $\mathbf{H}(\vec{u})$ stand for Fourier transforms of the (instantaneous) image, object, and speckle PSF, respectively. For each frequency we calculate the mean values and standard deviations of the power spectra:

$$\mathbf{C}_I(\vec{u}) \equiv \frac{\mathrm{var}\left(|\mathbf{I}(\vec{u})|^2\right)^{1/2}}{\left\langle |\mathbf{I}(\vec{u})|^2 \right\rangle} = \frac{|\mathbf{O}(\vec{u})|^2}{|\mathbf{O}(\vec{u})|^2} \frac{\mathrm{var}\left(|\mathbf{H}(\vec{u})|^2\right)^{1/2}}{\left\langle |\mathbf{H}(\vec{u})|^2 \right\rangle} = \frac{\mathrm{var}\left(|\mathbf{H}(\vec{u})|^2\right)^{1/2}}{\left\langle |\mathbf{H}(\vec{u})|^2 \right\rangle} \tag{5}$$

where $\langle . \rangle$ denotes average and $\mathrm{var}(.)$ denotes variance. We use the term "contrast", and denote it with letter *C* as is customary in research pertaining to speckle [4]. As can be appreciated from Equation (5) in the absence of noise the object disappears in $\mathbf{C}_I(\vec{u})$. With noise present in the data the object does not cancel out after the transformation but its influence is very small on the low-frequency part of $\mathbf{C}_I(\vec{u})$ which is the part where r_0 estimation must be performed. Models for $\left\langle |\mathbf{H}(\vec{u})|^2 \right\rangle$ and $\mathrm{var}\left(|\mathbf{H}(\vec{u})|^2\right)$ have been developed using the theory of partially-developed speckle [15]. Since the models depend only on *D*, λ and r_0 it is possible to estimate Fried's parameter by fitting theoretical templates to measured $\mathbf{C}_I(\vec{u})$.

Once r_0 is given the long-, and short-exposure (tip-tilt corrected) PSFs can be generated using the theory of Fried [13]. In this theory, the optical transfer function OTF, i.e., the Fourier transform of the PSF, for the two cases of long exposures and registered short exposures is given by:

$$\mathbf{H}_L(\vec{u}) = \mathbf{H}_0(\vec{u}) \times \mathbf{H}_{LE}(\vec{u}) \tag{6}$$

$$\mathbf{H}_S(\vec{u}) = \mathbf{H}_0(\vec{u}) \times \mathbf{H}_{SE}(\vec{u}) \tag{7}$$

where $\mathbf{H}_{LE}(\vec{u})$ represents the average long-exposure OTF of the atmosphere, $\mathbf{H}_{SE}(\vec{u})$ is the average short-exposure OTF of the atmosphere, $\mathbf{H}_L(\vec{u})$ and $\mathbf{H}_S(\vec{u})$ are the overall long- and short-exposure average OTFs (including the effect of the telescope diffraction). For a diffraction-limited circular aperture of diameter *D* we have:

$$\mathbf{H}_0(\vec{u}) = \frac{2}{\pi}\left[\arccos\left(\frac{\bar{\lambda} z u}{D}\right) - \frac{\bar{\lambda} z u}{D}\sqrt{1-\left(\frac{\bar{\lambda} z u}{D}\right)^2}\right] \tag{8}$$

where $u = |\vec{u}|$, $\bar{\lambda}$ is the average wavelength, and *z* is the distance from the exit pupil to the image plane.

Fried developed expressions for $\mathbf{H}_{LE}(\vec{u})$ and $\mathbf{H}_{SE}(\vec{u})$:

$$\mathbf{H}_{LE}(\vec{u}) = \exp\left[-3.44\left(\frac{\bar{\lambda} z u}{r_0}\right)^{5/3}\right] \tag{9}$$

$$\mathbf{H}_{SE}(\vec{u}) = \exp\left\{-3.44\left(\frac{\bar{\lambda} z u}{r_0}\right)^{5/3}\left[1-\alpha\left(\frac{\bar{\lambda} z u}{D}\right)^{1/3}\right]\right\} \tag{10}$$

where α is a parameter that varies between 1/2 when there are both intensity and phase variations across the collecting aperture and 1 when only phase distortions are present. By Fourier-transforming Equations (6) or (7) one obtains the average PSF $\langle \mathbf{h}(x,y) \rangle$.

To solve Equation (2) we need to know the probability density function of turbulent PSF $p(\mathbf{h})$. In this paper we present the equations for the statistics of intensity, what we call the "focal-plane" constraint, but we will also mention at this stage that it is possible to constrain the statistics of the PSF in pupil plane and in the Fourier plane [16].

With infinitesimally small detectors (pixels), exposure times and filter bandwidths one can model $p(\mathbf{h})$ as the exponential distribution [4]:

$$p(\mathbf{h}) = \prod_{k}^{K}\prod_{x}^{X}\prod_{y}^{Y} \frac{1}{\langle \mathbf{h}(x,y) \rangle} e^{-\frac{\mathbf{h}(k,x,y)}{\langle \mathbf{h}(x,y) \rangle}} \tag{11}$$

where K is the number of speckle frames and X and Y are the numbers of pixels in x and y directions. Speckle patterns in general will be integrated: spatially, temporally, and spectrally. To model these effects, use is made of the gamma PDF [4]:

$$p(\mathbf{h}) = \prod_{k}^{K}\prod_{x}^{X}\prod_{y}^{Y} \frac{1}{\Gamma(M)}\left(\frac{M}{\langle \mathbf{h}(x,y) \rangle}\right)^{M} \mathbf{h}(k,x,y)^{(M-1)} \exp\left\{-\frac{M\,\mathbf{h}(k,x,y)}{\langle \mathbf{h}(x,y) \rangle}\right\} \tag{12}$$

where M is the general integration parameter, a product of the spatial, spectral and temporal integration parameters [17].

In closing this section we also give an equation for the data-fidelity term in Equation (2). Under the assumption of spatially-stationary Gaussian noise with standard deviation σ we have:

$$p(\mathbf{i}|\mathbf{o},\mathbf{h}) = \left(\sigma\sqrt{2\pi}\right)^{-K\,X\,Y} \prod_{k}^{K}\prod_{x}^{X}\prod_{y}^{Y} \exp\left\{-\frac{\left[\mathbf{i}(k,x,y) - (\mathbf{o}\otimes\mathbf{h})(k,x,y)\right]^2}{2\sigma^2}\right\} \tag{13}$$

We assume $p(\mathbf{o})$ is a uniform distribution and solve the MAP problem using Equations (12) and (13).

3. DISTRIBUTION TESTING

Because real data contains both Poisson and readout components on top of speckle variability, the assumption of the gamma model for the integrated speckle was tested against a noise-free simulation. The simulation employs only one phase screen and assumes isoplanatic conditions (only global image motion). Scintillation effects are ignored.

Independent phase screens are generated using the classic FFT-based method [18], whereby an array of random numbers is filtered according to the von-Karman spectrum and then inverse Fourier-transformed. The outer scale was set to 25 m. We deliberately did not use subharmonics correction and we removed global tip/tilts from the wavefronts in order to have the same – in the statistical sense – speckles falling on a given pixel. Size of the telescope aperture was set to 50 cm and 256×256 pixel arrays were used for phase screens giving pupil sampling of 2 mm per pixel. Fried's parameter was set to 2 cm at 500 nm which is also the reference wavelength of the simulations. The phase screens were converted to phasors, multiplied by a circular aperture and embedded in an array of zeros of size 512×512 pixels. The field was then Fourier-transformed. Square of the modulus of the result gives the PSF. Pixel scale of the images is 49 μrad (Nyquist sampling at the shortest wavelength). The simulation is polychromatic: images corresponding to ten wavelengths between 500 and 700 nm are generated assuming linear wavefront scaling. The resulting ten PSFs are co-added and the result constitutes one polychromatic noise-free PSF. Additionally, five such PSFs were added to simulate temporal averaging. This binning size was chosen by trial-and-error with the goal to obtain similar values of integration parameter M across the field-of-view as in the SOR data. In the end, a sequence of 200 integrated images was generated out of 1000 instantaneous polychromatic frames.

The Kolmogorov-Smirnov [19,20] and Anderson-Darling [21] statistical tests were used to obtain quantitative confidence levels for the null hypothesis that a speckle sample from a given pixel comes from the gamma distribution. In both tests the test statistic D is a measure of distance between the empirical distribution function (EDF) - which is the proportion of the observed values that are less than or equal to a particular value - and the hypothesized cumulative density function (CDF). In the Kolmogorov-Smirnov test D is the maximum of the absolute difference between EDF and CDF, while in the Anderson-Darling test D corresponds to the weighted squared difference between EDF and CDF. If the null hypothesis - that CDF is the underlying distribution - is correct, EDF should be close to CDF and D should be close to zero. The result of the test, the p-value, gives the probability that a value of D at least as large as the one observed would have occurred if the null hypothesis were true. The greater the p-value the more confidence one can have in the null hypothesis. Usually, values higher than 0.05 are taken as strong evidence that a sample came from the hypothesized distribution (p-value is bounded between 0 and 1).

When all the parameters of a hypothesized CDF are specified a priori, there exist approximate formulas for the computation of the p-value. Unfortunately this was not the case here: both $\langle \mathbf{h}(x,y) \rangle$ and M in Equation (12) have to be estimated from the sample. Because of that the bootstrap simulation had to be used in order to obtain the p-values [22]. The parameters of the gamma distribution were estimated using the method of moments. In this approach, sample moments are equated to the unobservable population moments. Then the equations relating the distribution parameters to the population moments are solved. Specifically, computation of M follows as:

$$M = \frac{\langle \mathbf{h}(x,y) \rangle^2}{\mathrm{var}(\mathbf{h}(x,y))} \tag{14}$$

Computation of $\langle \mathbf{h}(x,y) \rangle$ is trivial. With both these parameters gamma CDF can be computed and the Kolmogorov-Smirnov and Anderson-Darling tests can be applied to the sample.

The bootstrap simulation is a Monte-Carlo approach to estimating the confidence intervals for the null hypothesis. The random variables with the hypothesized distribution are generated, and the parameters of the distribution are estimated from the simulated samples using the same method as for the observed sample. Again, the test statistic D is calculated. The result of the bootstrap method is the number of times the test statistic D calculated from the generated sample is greater than or equal to D calculated from the observed sample. This number divided by the total number of simulations gives the p-value. Gamma-distributed random variables were generated using the method of Marsaglia and Tsang [23]. Ten thousand samples of the same size as a given data set were generated. The

p-values were averaged for all pixels having the same distance from the center of the PSF. This is because the spectral component of parameter *M* increases with distance from the center (the spatial and temporal components are constant). One can explain it in the following way: *M* can be thought of as a number of speckles contributing to one pixel. Imagining a discrete set of increasing wavelengths, producing radially expanding PSFs, we see that stepping over wavelengths results in new speckles traversing a pixel under observation if it is away from the PSF center. The further a pixel is from the center the more speckles will traverse it (compare the sharp speckles close in to the smooth streaks further out from the center in the left panel of Figure 2).

The results of statistical testing are shown in Figure 1 for the distances of 0-30 pixels from the center. In almost all cases we obtained values higher than 0.3. This indicates that the gamma PDF provides a good model for the integrated speckle (spatially, temporally and spectrally).

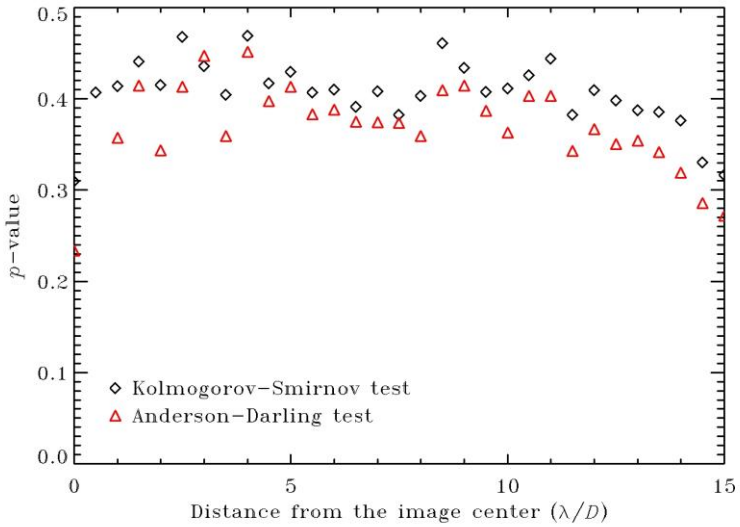

Fig. 1. Confidence levels, quantified by the K-S or A-D *p*-value, that the integrated speckle intensity is governed by the gamma PDF.

4. RESULTS

The model PDFs from Equations (12) and (13) were converted to negative log-likelihoods and, together with analytic gradients, inserted into a Variable Metric with Limited Memory (VMLM) optimizer [24]. I-band (800-900 nm) observations of the bright single star HR2219 (Figure 2, top left panel) have been obtained with the 3.5 m telescope at the Starfire Optical Range with adaptive optics switched off (but with the tip/tilt system switched on). Thousand frames were recorded, with exposure time set to 10 ms. We obtained $D/r_0 = 34$ from the Fourier contrast method.

To execute our MFBD on real data we needed to know the integration parameter *M* to be plugged into Equation (12). The estimation of *M* for spatial-only integration is straightforward when one knows the auto-correlation function of speckle and pixel shape [4,17]. Also, we conjecture that estimation of spectral *M* could be done easily under the assumption of rectangular filter and the similarity of spatial and spectral auto-correlation functions (the latter will be the scaled version of the former with the scaling parameter depending on the distance from the image center; see the text preceding Figure 1). Both these components of the total *M* would have to be computed only once for a given telescope-camera-filter combination. The problematic part is the estimation of temporal *M*. Use will have to be made of the analytical temporal auto-correlation function which has a dependency on the vertical profile of wind velocity [25].

Before we attempt a fully reference-less, analytical computation of spatial-spectral-temporal *M*, we estimate it from the combination of real data statistics and corresponding noise-less simulation. Figure 2 shows *M* (in the right panels) of either real speckle images (top left panel) or the simulated ones (bottom left panel). Simulated data

corresponding to SOR parameters (wavelength, filter bandwidth, pixel size, telescope diameter, etc.) was generated using the approach described in Section 3, but with subharmonics correction of the phase-screens. Computation of *M* at each location in the PSF was done by the means of Equation (14). Note how the *M* image for real speckles is only valid where the SNR is high, i.e., where the speckle fluctuations are higher than noise. We used the *M* image of simulated speckles to scale *M* of SOR data by a constant value to correct for the difference in the integration time between the simulated (instantaneous exposure) and the real (10 ms) images. In such way we have been able to use the gamma prior for the whole field-of-view which was not possible in the case of the real *M* image only (Figure 2, top right panel) because of noise.

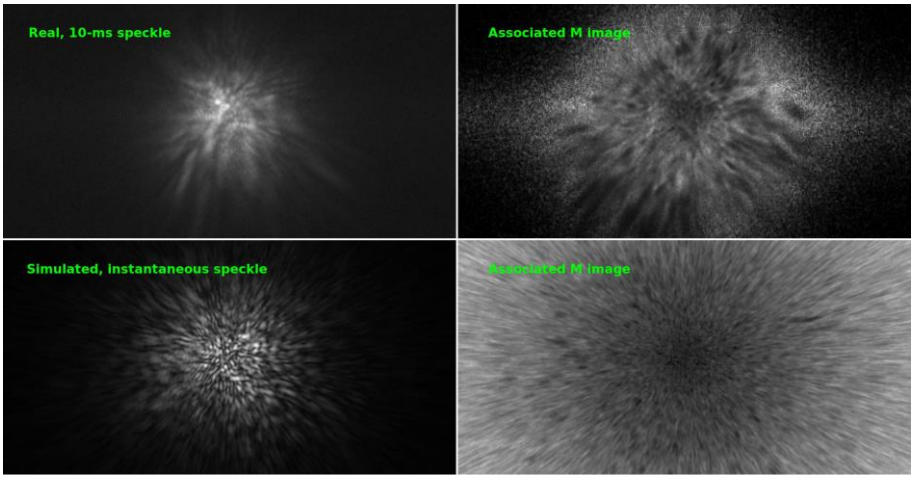

Fig 2. Top left: a real speckle image taking with the 3.5 m SOR telescope, exposure time equal 10 ms, spectral bandwidth from 800 to 900 nm, pixel size 80.5 nrad. Top right: the associated *M* image. Bottom left: a simulated speckle image for the same telescope, instantaneous exposure time, bandwidth from 800 to 900 nm, pixel size equal 80.5 nrad. Bottom right: the corresponding *M* image.

Speckle images from the single star HR2219 were used as PSFs. They were convolved with a schematic representation of the Hubble Space Telescope (HST, Figure 3) which acted as the true object. The resulting images were corrupted with Gaussian noise of standard deviations equal to 1 or 5 counts.

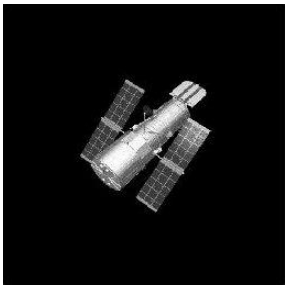

Fig 3. True object used for the simulations.

Multi frame blind deconvolution with gamma PSF prior was used to deconvolve the simulated data. Results are shown in Figure 4. Reconstructions show significantly enhanced contrast with respect to either a single frame or to the shift-and-add image. Figure 5 shows evolution with the number of iterations of the peak signal-to-noise ratio (PSNR) defined as:

$$\mathrm{PSNR} = 10\log_{10}\frac{L^2}{\mathrm{MSE}} \tag{15}$$

where L is the dynamic range of the image. PSNR is calculated using the mean squared error (MSE) which compares a particular reconstruction **A** with the reference true image **B**:

$$\mathrm{MSE} = \frac{1}{XY}\sum_{x=1}^{X}\sum_{y=1}^{Y}\left(\mathbf{A}(x,y)-\mathbf{B}(x,y)\right)^2 \tag{16}$$

From Figure 5 it is clear that use of the gamma distribution prior on the PSF prevents noise amplification in the reconstruction.

Finally, in Figure 6 we compare the estimated PSFs with the real ones used for the simulations. Our estimates follow the general morphology and shape of the real PSFs in terms of size, elongation and maximum-peak positions but lack the same high-frequency content.

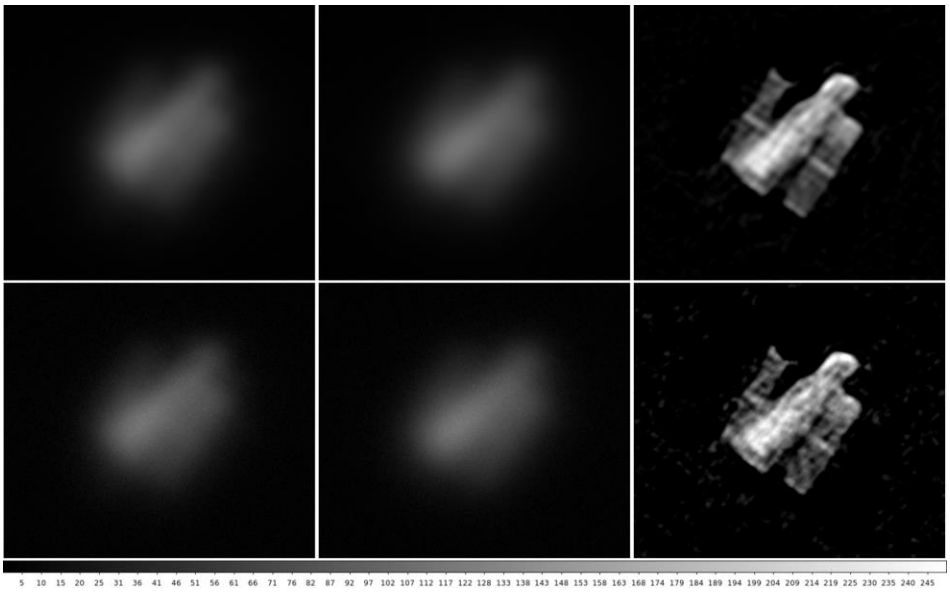

Fig 4. Top row: case of readout noise with σ = 1. Bottom row: case of readout noise with σ = 5. Left column: single frames. Middle column: shift-and-add images. Right column: final reconstructions. Linear scale from 0 to 250 is the same in all panels.

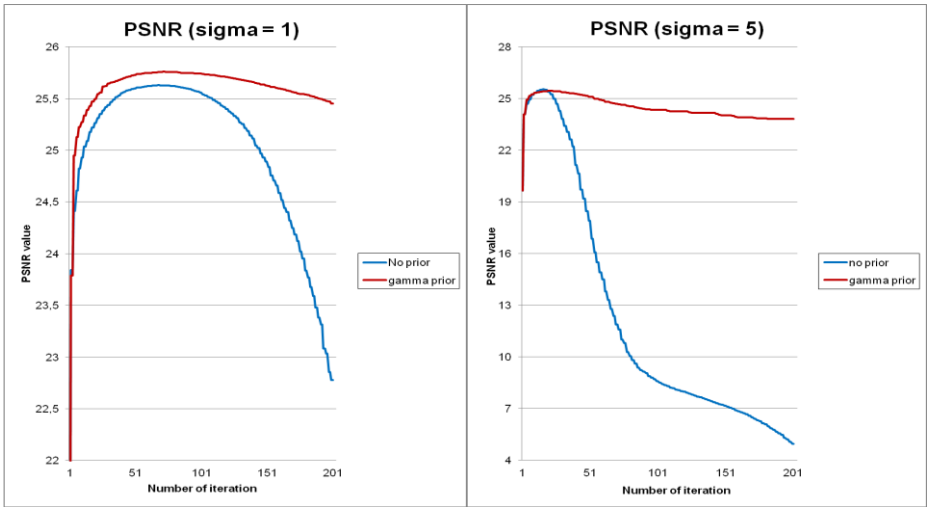

Fig 5. PSNR values vs. number of iterations for two noise levels.

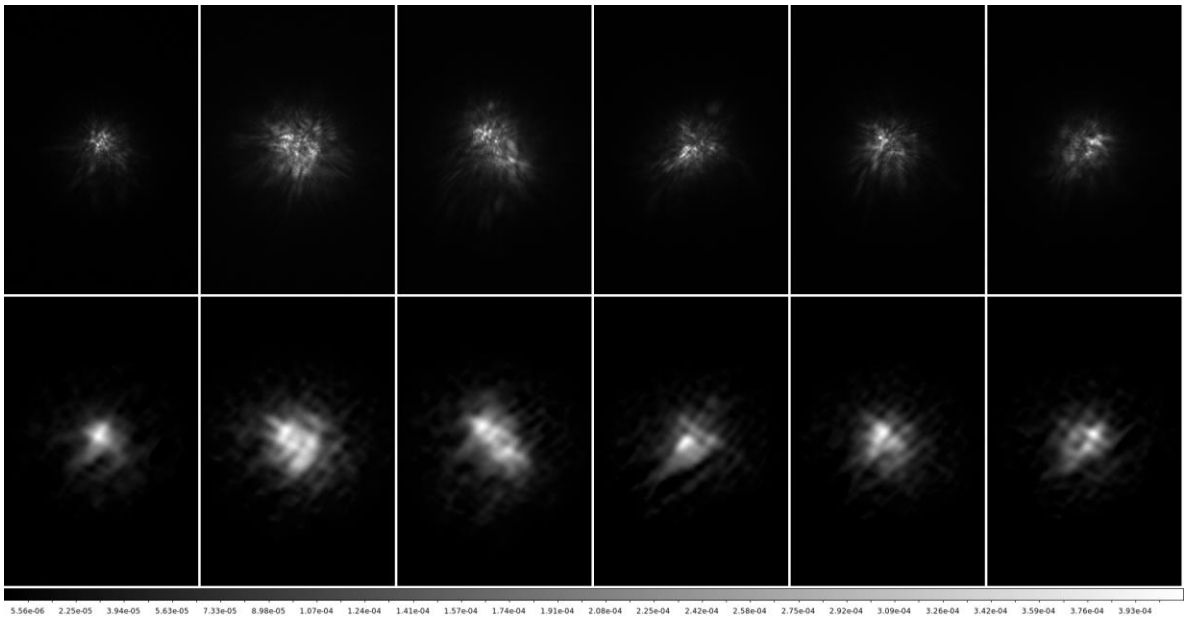

Fig 6. Top row: real speckle images used as PSFs. Bottom row: Estimated PSFs from MFBD.

5. OUTLOOK

Currently, we are estimating the integration parameter *M* using the PSFs and simulations. To satisfy the "no reference" goal of the project we will have to estimate *M* analytically with the assumed spatial, spectral and temporal auto-correlations. The validity of these assumptions will have to be tested against real data. Temporal and spectral integration effects are particularly interesting. Modeling of them has been attempted in the context of speckle interferometry but the resulting formulas are rather complex and have dependencies on several parameters which cannot be easily obtained from the data, like phase variance [26]. We hope to provide an alternative, simple description of the effect of integration on various speckle statistics. Subsequently, we will test PSF priors expressed in the pupil plane and in the Fourier plane [16].

ACKNOWLEDGEMENTS

Effort sponsored by U.S. Air Force Office of Scientific Research, Air Force Material Command, under grant FA8655-12-1-2115, and the Spanish Ministry of Science under grant AyA2008-01225. The U.S. Government is authorized to reproduce and distribute reprints for Governmental purpose notwithstanding any copyright notation thereon.

REFERENCES

[1] L. M. Mugnier, T. Fusco, and J.-M. Conan, "MISTRAL: a myopic edge-preserving image restoration method, with application to astronomical adaptive-optics-corrected long-exposure images," J. Opt. Soc. Am. A 21, 1841-1854 (2004).

[2] R. Baena Gallé, J. Núñez, and S. Gladysz, "Extended object reconstruction in adaptive-optics imaging: the multiresolution approach," Astronomy & Astrophysics, 555, A69-A84, (2013)..

[3] J. C. Dainty, "Stellar speckle interferometry", in Laser Speckle and Related Phenomena, edited by J. C. Dainty, Springer Verlag, Heidelberg, 2nd Edition (1984).

[4] J. W. Goodman, "Speckle phenomena in optics: theory and applications," (Roberts & Company, 2006).

[5] D. W. Tyler, "Deconvolution of adaptive optics image data," Proceedings of the Center for Adaptive Optics, (2001).
[6] T. J. Schulz, "Multiframe blind deconvolution of astronomical images," J. Opt. Soc. Am. A 10, 1064-1073 (1993).
[7] D. G. Sheppard, B. R. Hunt, and M. W. Marcellin, "Iterative multiframe superresolution algorithms for atmospheric-turbulence-degraded imagery," J. Opt. Soc. Am. A 15, 978-992 (1998).
[8] C. L. Matson, K. Borelli, S. Jefferies, C. C. Beckner, Jr., E. K. Hege, and M. Lloyd-Hart, "Fast and optimal multiframe blind deconvolution algorithm for high-resolution ground-based imaging of space objects," Appl. Opt. 48, A75-A92 (2009).
[9] J. Nagy and V. Mejia-Bustamante, "MFBD and the local minimum trap," Proceedings of the AMOS Conference, 2009, Ed.: S. Ryan, The Maui Economic Development Board, p.E10
[10] L. Blanco and L. M. Mugnier, "Marginal blind deconvolution of adaptive optics retinal images," Opt. Express 19, 23227-23239 (2011).
[11] L. M. Mugnier, C. Robert, J.-M. Conan, V. Michau, and S. Salem, "Myopic deconvolution from wave-front sensing," J. Opt. Soc. Am. A 18, 862-872 (2001).
[12] A. MacDonald, S. C. Cain, and E. E. Armstrong, "Maximum a posteriori image and seeing condition estimation from partially coherent two-dimensional light detection and ranging images," Opt. Eng. 45, 086201-1-13 (2006).
[13] D. L. Fried, "Optical resolution through a randomly inhomogeneous medium for very long and very short exposures," J. Opt. Soc. Am. 56, 1372-1379 (1966).
[14] O. von der Lühe, "Estimating Fried's parameter from a time series of an arbitrary resolved object imaged through atmospheric turbulence," J. Opt. Soc. Am. A 1, 510-519 (1984).
[15] S. Gladysz, R. Baena Gallé, R. Johnson, and L. Kann, "Image reconstruction of extended objects: demonstration with the Starfire Optical Range 3.5m telescope," Proceedings of SPIE, Volume 8535, 85350M-1-13 (2012).
[16] R. Baena Gallé, S. Gladysz, L. Mugnier, V. Gudimetla, R. Johnson, and L. Kann, "Physically-constrained Multi-frame Blind Deconvolution," in Imaging and Applied Optics, J. Christou and D. Miller, eds., OSA Technical Digest (online) (Optical Society of America, 2013), paper JW2A.3
[17] S. E. Skipetrov, J. Peuser, R. Cerbino, P. Zakharov, B. Weber, and F. Scheffold, "Noise in laser speckle correlation and imaging techniques," Opt. Express 18, 14519-14534 (2010).
[18] B. L. McGlamery, "Computer simulation studies of compensation of turbulence degraded images," in Image Processing, J. C. Urbach, ed., Proc. SPIE 74, 225-233 (1976).
[19] A. N. Kolmogorov, "Sulla determinazione empirica di una legge di distribuzione," Giornale dell' Istituto Italiano degli Attuari 4, 83-91 (1933).
[20] N. V. Smirnov, "Table for estimating the goodness of fit of empirical distributions," The Annals of Mathematical Statistics, 19, 279-281 (1948).
[21] T. W. Anderson and D. A. Darling, "Asymptotic theory of certain "goodness-of-fit" criteria based on stochastic processes," Annals of Mathematical Statistics 23, 193-212 (1952).
[22] S. Gladysz, J. C. Christou, L. W. Bradford, and L. C. Roberts, Jr., "Temporal variability and statistics of the Strehl ratio in adaptive-optics images," PASP 120,1132-1143 (2008).
[23] G. Marsaglia and W. Tsang, "A simple method for generating gamma variables," ACM Transactions on Mathematical Software 26, 363-372 (2000).
[24] E. Thiebaut, "Optimization issues in blind deconvolution algorithms," in Astronomical Data Analysis II, SPIE Vol. 4847, 174-183 (2002).
[25] F Roddier, J M Gilli and G Lund, "On the origin of speckle boiling and its effects in stellar speckle interferometry," J. Optics 13, 263-271 (1982).
[26] J. Ohtsubo, "Effects of finite spectral bandwidth and focusing error on the transfer function in stellar speckle interferometry," J. Opt. Soc. Am. A 2, 667-673 (1985).